A R C H I V E S O F M E T A L L U R G Y A N D M A T E R I A L S
Volume 59 2014 Issue 1
DOI: 10.2478/amm-2014-0045

L. BLACHA*, S. GOLAK*, A. JAKOVICS**, A. TUCS**

KINETIC ANALYSIS OF ALUMINIUM EVAPORATION FROM THE Ti-6Al-7Nb ALLOY

ANALIZA KINETYCZNA PROCESU PAROWANIA ALUMINIUM ZE STOPU Ti-6Al-7Nb

In the present paper, kinetics of aluminium evaporation from the Ti-6Al-7Nb alloy during smelting by means of the VIM method at 5 to 1000 Pa has been discussed. To determine the liquid titanium meniscus area and the liquid titanium mean velocity for the experimental conditions of the study, a methodology based on the coupled model of the electromagnetic field and the hydrodynamic field of liquid metal was applied.
Keywords: kinetic analysis, evaporation, Ti-6Al-7Nb alloy, liquid titanium meniscus area, liquid titanium mean velocity

W prezentowanej pracy omówiono kinetykę procesu odparowania aluminium ze stopu Ti-6Al.-7Nb wytapianego metodą VIM w zakresie ciśnień od 5 do 1000Pa. Do wyznaczenia powierzchni menisku ciekłego tytanu oraz średniej prędkości ciekłego tytanu wykorzystano model matematyczny procesu topienia i nagrzewania ciekłego metalu w piecu indukcyjnym uwzględniający sprzężenie pola elektromagnetycznego i pola hydrodynamicznego ciekłego metalu.

1. Introduction

Titanium alloys belong to a group of the most modern constructional and functional materials. They are light and designed for e.g. high-temperature application. A growing role and industrial importance of these materials can be clearly demonstrated by comparison to properties of other metal alloys. For instance, density of titanium alloys is equal to about 50% of steel density. Therefore, masses of various system elements made of these alloys can be by half smaller than those of the same steel element types. Strengths of titanium alloys, far higher than strengths of many alloy steels, highly promote these materials considering the strength to mass density ratio. Moreover, it should be noted than titanium alloys show better resistance to corrosion and oxidation compared to stainless steels, which also markedly improves their applicability. Titanium alloy smelting is mainly performed using VIM or VAR methods. However, during melting and casting of these materials, evaporation of their volatile matter can occur. For instance, during Ti-Al-V or Ti-Al-Nb smelting intense aluminium evaporation is observed [1-6]. Similarly, during Ti-Al-Mn alloy smelting, a component subjected to intense evaporation is manganese [7]. To prevent this, knowledge on the process kinetics is necessary as for various vacuum ranges in a furnace, the stage that controls its rate may change. In the present paper, kinetics of aluminium evaporation from the Ti-6Al-7Nb alloy during smelting by means of the VIM method at 5 to 1000 Pa has been discussed.

2. Research methodology

In Table 1, a chemical composition of Ti-6Al-7Nb alloy used for smelting experiments is presented.

TABLE 1
Chemical composition of the investigated alloy

Alloy type	Basic alloy component fractions, %mass				
	Al	Nb	Fe	Ta	Ti
Ti-6Al-7Nb	5.5 – 6.5	6.5 – 7.5	$\leqslant 0.25$	$\leqslant 0.5$	The other fraction

The experiments were performed using a one-chamber VIM 20-50 vacuum induction furnace manufactured by SECO-WARWICK. At the beginning of each experiment, an alloy sample (about 1000 g) was placed in a graphite melting pot located in the induction coil of the furnace. After closing the furnace chamber, a precisely specified vacuum was generated using diffusive and Roots pumps. When the required vacuum level was reached, the melting pot was heated up to the set temperature and the metal bath was held at it for 600 sec. During the experiment, alloy samples were collected and subjected to a further chemical analysis. All experiments were performed at 5-1000 Pa and 1972-2023 K.

3. Results

The overall mass transfer coefficient in the analysed evaporation process is determined by the following equation [8]:

* SILESIAN UNIVERSITY OF TECHNOLOGY, FACULTY OF MATERIALS ENGINEERING AND METALLURGY, 40-019 KATOWICE, 8 KRASINSKIEGO STR., POLAND
** UNIVERSITY OF LATVIA, LABORATORY FOR MATHEMATICAL MODELLING OF ENVIRONMENTAL AND TECHNICAL PROCESSES, LV-1002 RIGA, ZELLU STR. 8, LATVIA

$$\frac{1}{k} = \frac{1}{\beta^l} + \frac{1}{\phi k^e} + \frac{RT}{\phi \beta^g} \tag{1}$$

where:

$$\phi = \frac{p_i^o \cdot \gamma_i \cdot M_m}{\rho_m} \tag{2}$$

where:β^l – mass transfer coefficient in the liquid phase,

β^g – mass transfer coefficient in the gaseous phase,

k_e – evaporation rate constant,

R – gas constant,

T – temperature,

M_m;ρ_m – respectively: molar mass and density of the basic alloy component, titanium,

p_i^0;γi – respectively: aluminium vapour pressure over pure bath and its reactivity coefficient in liquid alloy.

In order to determine the overall mass transfer coefficient value for aluminium based on the experimental data, the following equation was applied:

$$2.303 \log \frac{C_{Al}^t}{C_{Al}^o} = -k_{Al} \cdot \frac{F}{V}(t - t_o) \tag{3}$$

where:

C_{Al}^t – aluminium concentration in the alloy after time t,

C_{Al}^0 – initial aluminium concentration,

F – evaporation area (the interface),

V – liquid metal volume,

(t – t_o) – process duration.

The equation (3) shows that a parameter that meaningfully affects the k_{Al} value is the evaporation area F. In most cases, this parameter is assumed by Authors studying the evaporation kinetics of inductively stirred metal bath volatile matter to be the cross-section areas of the melting pot. This may cause a pronounced calculation error as under such hydrodynamic conditions, a meniscus is formed with a far larger surface than the inner cross-section of the melting pot. To determine the liquid titanium meniscus area for the experimental conditions of the study, a methodology based on the coupled model of the electromagnetic field and the hydrodynamic field of liquid metal was applied. A detailed description of the method can be found further in the paper. In Fig. 1, a shape of the titanium bath in the electromagnetic field is presented. In this case, the meniscus surface area was 0.0068 m^2 and the cross-section area of the experimental melting pot was 0.0063 m^2.

In Table 2, values of the experimental coefficient k_{Al}, determined using the equation (3), are presented.

In order to determine the ratio of resistance related to mass transfer in liquid Ti-Al-Nb alloy to the overall evaporation process resistance, values of mass transfer coefficient, $ß_{Al}^l$, must be known. They were estimated using the Machlin equation which describes mass transfer in the inductively stirred liquid metal phase. The equation is as follows [9]:

$$\beta_{Al}^l = \left(\frac{8 D_{Al} \cdot v_m}{\pi \cdot r_m}\right)^{\frac{1}{2}} \tag{4}$$

where:

v_m – near-surface velocity of inductively stirred liquid metal,

r_m – radius of the liquid metal surface (assumed to be the melting pot inner radius),

D_{Al} – Al diffusion coefficient in liquid alloy.

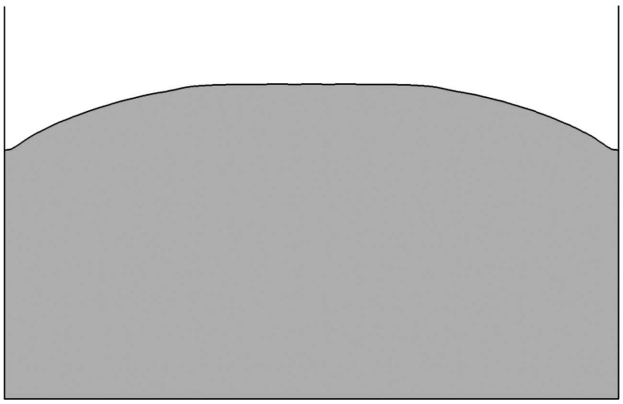

Fig. 1. Titanium bath shape in the electromagnetic field

According to many Authors, the v_m value does not depend on the type of inductively stirred alloy or the electrical parameters of the furnace operation and it is 0.1 $m \cdot s^{-1}$ for devices where up to 1 Mg of metal is smelted. However, many studies have shown that this parameter depends on a lot of factors, i.e. metal density and viscosity as well as the electrical parameters of furnace operation [10]. To determine the v_m value, the following empirical equation can be used [11]:

$$v_m = v_1 + (v_2 - v_1) \cdot \frac{(T - T_1)}{300} \tag{5}$$

In the present paper, to determine a liquid titanium mean velocity, a mathematical model of liquid metal melting and heating in the induction furnace, considering the electromagnetic field and hydrodynamic field coupling, was applied.

The essential problem that impedes modelling of the process is the fact that the electromagnetic field affects the hydrodynamic field of liquid metal bath, changing its surface shape. The shape changes, affecting the electromagnetic field distribution, require calculations of the electromagnetic and hydrodynamic fields for each simulation step [12, 13] or at a frequency sufficient for maintaining the current field distribution by means of the mathematical extrapolation [14, 15].

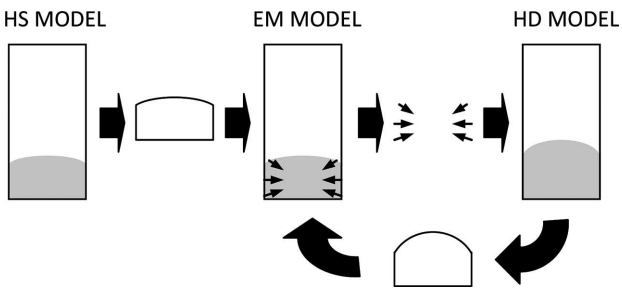

Fig. 2. Simulation algorithm diagram

In Fig. 2, the study simulation algorithm diagram is presented. The simulation begins with determination (by hydrostatic calculations) of the initial metal bath shape without the electromagnetic field based on the liquid titanium surface tension and the contact angle of the graphite melting pot wetted by liquid titanium. Then, the obtained liquid metal shape is

an input parameter for the electromagnetic model that ensures determination of the distribution of electromagnetic force field acting on liquid metal. A two-dimensional, axially symmetric electromagnetic model was based on a commonly used equation [16, 17] where the magnetic vector potential is applied:

$$\nabla \times \left(\frac{1}{\mu}\nabla \times \mathbf{A}\right) + \mathrm{j}\omega\sigma\mathbf{A} = \mathbf{J_s} \tag{6}$$

where: μ, σ – magnetic permeability and conductivity of titanium,

ω – angular frequency,

$\boldsymbol{J}_\mathbf{s}$ – source current density.

Based on the distribution of potential **A**, determined using the finite element method, distribution of magnetic induction (***B***) (7), eddy current densities (***I***) (8) and the density of electromagnetic force that acts on liquid metal ($\boldsymbol{f}_\mathbf{e}$)(9) can be determined:

$$\mathbf{B} = \nabla \times \mathbf{A} \tag{7}$$

$$\mathbf{J} = \mathrm{j}\omega\sigma\mathbf{A} \tag{8}$$

$$\mathbf{f_e} = \frac{1}{2}Re\,(\mathbf{J} \times \mathbf{B}^*) \tag{9}$$

The next step includes hydrodynamic calculations which, based on the VOF method, allows for determination of a change in the bath surface shape that, again, is the input parameter for the electromagnetic model. The model was based on the solution (using the finite volume method) of the set of continuity and Navier-Stokes equations for incompressible fluid:

$$\frac{\partial\rho}{\partial t} + \nabla\,(\rho\mathbf{v}) = 0 \tag{10}$$

$$\frac{\partial\alpha}{\partial t} + \nabla\,(\alpha\mathbf{v}) = 0 \tag{11}$$

$$\alpha\rho_m\left(\frac{\partial\mathbf{v}}{\partial t} + \mathbf{v}\cdot\nabla\mathbf{v}\right) = -\nabla p + \alpha\eta_{eff}\nabla^2\mathbf{v} + \mathbf{f_e} \tag{12}$$

where: v – velocity,

η_{eff} – titanium effective viscosity including turbulent viscosity determined using the popular k-epsilon model [18, 19],

ρ_m – titanium density,

p – pressure,

α – titanium volume fraction.

To maintain calculation stability, the simulation cycle was performed within a relatively short timeframe of 10^{-4} sec. A condition of simulation completion was lack of changes in liquid metal surface shape and its volumetric flow field. In Fig. 3, a sample, calculated liquid titanium velocity field for T= 2023 K is presented. Mean near-surface velocities, determined using the above model, were 0.135 to 0.149 ms^{-1}.

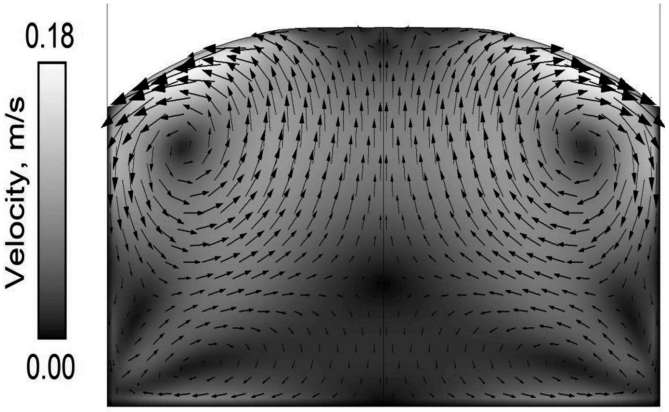

Fig. 3. Liquid titanium velocity field for T = 2023 K

TABLE 2

Estimated values of coefficients k_{Al}, $k^{e'}_{Al}$, β^{l}_{Al}

Test no.	Temperature, K	Pressure, Pa	Final Al concentration %mass	Coefficient k_{Al}, $\mathrm{m{\cdot}s^{-1}}$	Coefficient β^{l}_{Al}, $\mathrm{m{\cdot}s^{-1}}$	Coefficient $k^{e'}_{Al}$, $\mathrm{m{\cdot}s^{-1}}$
1	1973	1000	3.94	$2.04{\cdot}10^{-5}$	$3.02{\cdot}10^{-4}$	$5.43{\cdot}10^{-5}$
2	1973	100	3.77	$2.15{\cdot}10^{-5}$	$3.02{\cdot}10^{-4}$	$5.43{\cdot}10^{-5}$
3	1973	50	3.67	$2.29{\cdot}10^{-5}$	$3.02{\cdot}10^{-4}$	$5.43{\cdot}10^{-5}$
4	1973	10	3.66	$2.33{\cdot}10^{-5}$	$3.02{\cdot}10^{-4}$	$5.43{\cdot}10^{-5}$
5	1973	5	3.34	$2.49{\cdot}10^{-5}$	$3.02{\cdot}10^{-4}$	$5.43{\cdot}10^{-5}$
6	1998	1000	3.88	$2.24{\cdot}10^{-5}$	$3.47{\cdot}10^{-4}$	$6.85{\cdot}10^{-5}$
7	1998	100	3.69	$2.32{\cdot}10^{-5}$	$3.47{\cdot}10^{-4}$	$6.85{\cdot}10^{-5}$
8	1998	50	3.63	$2.40{\cdot}10^{-5}$	$3.47{\cdot}10^{-4}$	$6.85{\cdot}10^{-5}$
9	1998	10	3.56	$2.57{\cdot}10^{-5}$	$3.47{\cdot}10^{-4}$	$6.85{\cdot}10^{-5}$
10	1998	5	3.30	$2.86{\cdot}10^{-5}$	$3.47{\cdot}10^{-4}$	$6.85{\cdot}10^{-5}$
11	2023	1000	3.86	$2.34{\cdot}10^{-5}$	$3.96{\cdot}10^{-4}$	$8.59{\cdot}10^{-5}$
12	2023	100	3.62	$2.42{\cdot}10^{-5}$	$3.96{\cdot}10^{-4}$	$8.59{\cdot}10^{-5}$
13	2023	50	3.57	$2.54{\cdot}10^{-5}$	$3.96{\cdot}10^{-4}$	$8.59{\cdot}10^{-5}$
14	2023	10	3.48	$2.79{\cdot}10^{-5}$	$3.96{\cdot}10^{-4}$	$8.59{\cdot}10^{-5}$
15	2023	5	3.19	$3.00{\cdot}10^{-5}$	$3.96{\cdot}10^{-4}$	$8.59{\cdot}10^{-5}$

In order to determine the aluminium diffusion coefficient in the liquid phase, the equation [20] was applied:

$$D_{Al} = 10^{-8} \exp\left[\frac{250000}{R}\left(\frac{1}{1925} - \frac{1}{T}\right)\right] \quad (13)$$

Values of aluminium mass transfer coefficient in the liquid phase, determined using the equation (3), are presented in Table 2.

To determine the ratio of resistance related to the act of evaporating on the metal bath surface to the overall resistance of the process, the k^e coefficient must be known. In this case, values estimated by the paper Authors using the Langmuir-Knudsen equation [6] were applied.

In Table 2, estimated values of substitutional evaporation rate constant, $k^{e'}$, determined using the following equation, are also presented:

$$k^{e'} = k^e \cdot \phi \quad (14)$$

For calculations, the coefficient of aluminium activity (γ_{Al}) in the alloy was assumed to be 0.09-0.1. The values of coefficient k^{ie} allowed for estimation of the ratio of resistance related to the act of evaporating on the metal bath surface to the overall resistance of the process.

4. Discussion on results

Based on the experimental results, it can be demonstrated that decrease in the system working pressure is accompanied by aluminium loss increase. For the tests performed at 5 Pa, the final fraction of this metal in the alloy dropped to below 4%mass with the initial fraction of 5.5 mass%. At the same time, the aluminium overall mass transfer coefficient increased from 2.03 10^{-5} to 3.46 10^{-5} ms^{-1}, which is illustrated by the data in Fig. 4. In Fig. 5, sample $k_{Al}\beta^l_{Al}$ and $k^{e'}_{Al}$ values versus temperature are presented. For all the pressure values, they are ordered as follows:

$$k_{Al} < \beta^l_{Al} < k^{e'}_{Al} \quad (15)$$

The obtained k_{Al}, $k^{e'}_{Al}$ and β^l_{Al} values were used for specifying the stages that determine the investigated process. The ratio of mass transfer resistance in the liquid phase was determined using the following equation:

$$U_l = \frac{\frac{1}{\beta^l_{Al}}}{\frac{1}{k_{Al}}} \cdot 100\% \quad (16)$$

and, analogically, the resistance related to the act of evaporating is:

$$U_e = \frac{\frac{1}{k^{e'}_{Al}}}{\frac{1}{k_{Al}}} \cdot 100\% \quad (17)$$

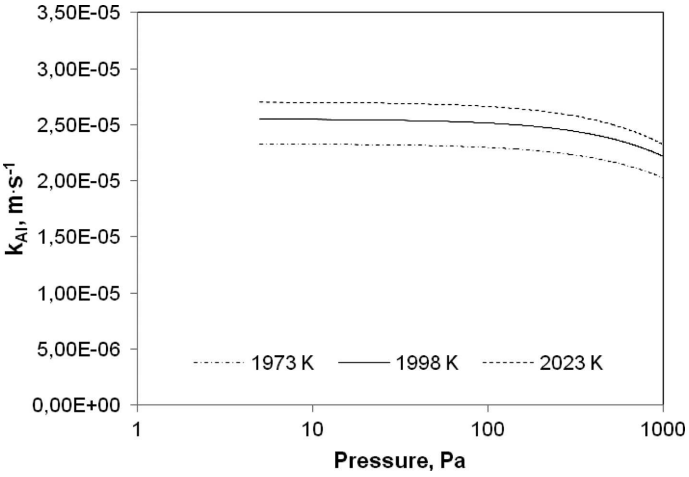

Fig. 4. Changes in the overall mass transport coefficient, k_{Al}, depending on the working pressure in the furnace

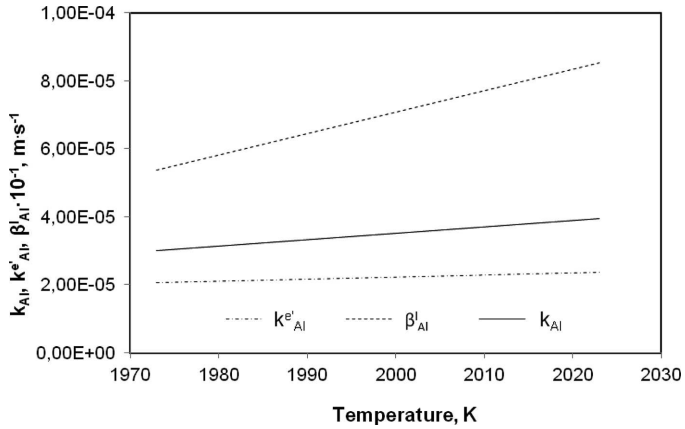

Fig. 5. Values of the k_{Al}, β^l, $k^{e'}$ values versus temperature – p = 1000Pa

The performed analysis revealed that for the entire pressure range, the ratio of resistance related to mass transfer in the liquid phase did not exceed 9%. The ratio of resistance related to the act of evaporating was as follows: 27 to 45% (Fig. 6), while the ratio of resistance related to mass transfer in the gaseous phase was over 45% of the overall process resistance (Fig. 7).

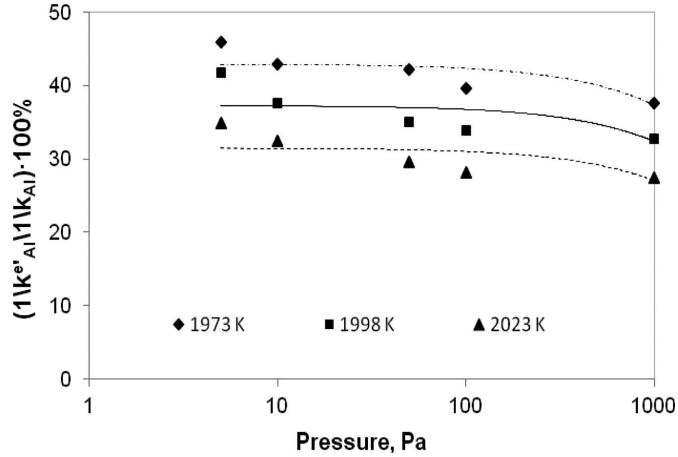

Fig. 6. Ratio of resistance related to the act of evaporating to the overall process resistance, depending on pressure

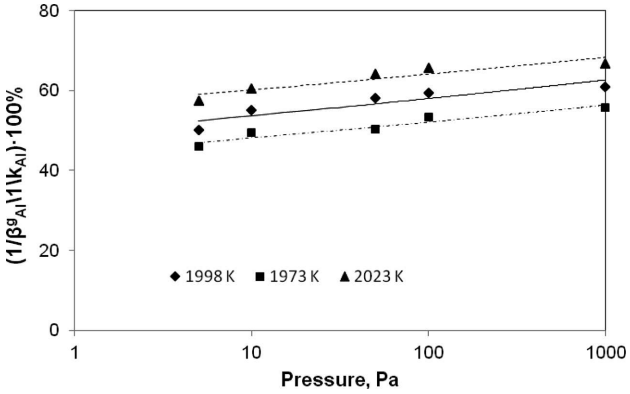

Fig. 7. Ratio of resistance related to mass transfer in the gaseous phase to the overall process resistance, depending on pressure

The summary ratio of resistance related to the act of evaporating and mass transfer in the gaseous phase was 90-95% (Fig. 8). This means that the two processes determine the rate of aluminium evaporation from Ti-6Al-7Nb.

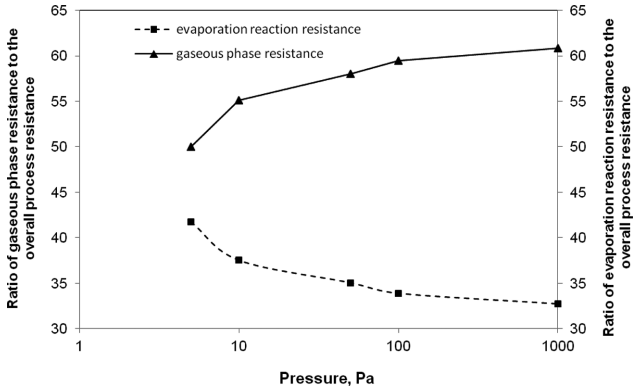

Fig. 8. Ratio of the summary resistance related to mass transfer in the gaseous phase and the act of evaporating to the overall process resistance, depending on pressure

5. Conclusion

Based on the investigations on aluminium evaporation from the Ti-6Al-7Nb alloy, it has been demonstrated that:

- ✓ The evaporation rate is determined by both the act of evaporating and the mass transfer in the gaseous phase.
- ✓ The summary ratio of process resistance related to these stages is about 90-95%.
- ✓ The ratio of resistance related to mass transfer in the liquid phase to the overall process resistance is lower than 10%.
- ✓ Thus, a factor that ensures reduction in disadvantageous aluminium evaporation from the investigated alloy is conducting the process at higher working pressures.

REFERENCES

[1] Y. Su, J. Guo, J. Jia, G. Liu, Y. Liu, Composition control of a Ti-Al melt during the induction skull melting process, Journal of Alloys and Compounds **334**, 261-266 (2002).

[2] G. Siwiec, Elimination of aluminum during the process of Ti-6Al-4V melting in a vacuum induction furnace, Archives of Metallurgy and Materials **57** (4), 951-956 (2012).

[3] L. Blacha, G. Siwiec, B. Oleksiak, Loss of aluminium during the process of Ti-Al-V alloy smelting in a vacuum induction melting (VIM) furnace, Metalurgija **52** (3), 301-304 (2013).

[4] G. Siwiec, The kinetics of aluminium evaporation from the Ti-6Al-4V alloy, Archives of Metallurgy and Materials **58** (4), 1155-1160 (2013).

[5] G. Siwiec, J. Mizera, D. Jama, A. Szmal, The effects of temperature on the kinetics of aluminium evaporation from the Ti-6Al-4V alloy, Metalurgija **53** (2), 225-227 (2014).

[6] L. Blacha, J. Mizera, P. Folęga, The effects of mass transfer in the liquid phase on the rate of aluminium evaporation from the Ti-6Al-7Nb alloy, Metalurgija **53** (4), 51-54 (2014).

[7] L. Blacha, R. Burdzik, A. Smalcerz, T. Matuła, Effects of pressure on the kinetics of manganase evaporation from the OT 4 alloy, Archives of Metallurgy and Materials **58** (1), 197-201 (2013).

[8] J. Łabaj, Kinetics of coper evaporation from the Fe-Cu alloys under reduced pressure, Archives of Metallurgy and Materials **57** (1), 165-172 (2012).

[9] C. Kolmasiak, Kinetics of chromium evaporation from heat-resisting steel under reduced pressure, Metalurgija **51** (3), 317-320 (2012).

[10] L. Blacha, J. Łabaj, Factors determining the rate of process of metal bath components evaporation, Metalurgija **51** (4), 529-533 (2012).

[11] J. Guo, G. Liu, Y. Su, H. Ding, J. Jia, H. Fu, Evaporation of multi-components in Ti-25Al-25Nb melt during induction skull melting process, Transactions of Nonferrous Metals Society of China **12** (4), 587-591 (2002).

[12] S. Spitans, A. Jakovics, E. Baake, B. Nacke, Numerical modelling of free surface dynamics of conductive melt in the induction crucible furnace, Magnetohydrodynamics **46** (4), 425-436 (2010).

[13] S. Spitans, A. Jakovics, E. Baake, B. Nacke, Numerical modelling of free surface dynamics of melt in an alternate electromagnetic field, Magnetohydrodynamics **47** (4), 385-397 (2011).

[14] S. Golak, R. Przyłucki, The optimization of an inductor position for minimization of a liquid metal free surface, Przeglad Elektrotechniczny **84** (11), 163-164 (2008).

[15] S. Golak, R. Przyłucki, A simulation of the coupled problem of magnetohydrodynamics and a free surface for liquid metals, Transactions WIT Transactions on Engineering Science **56**, 67-76 (2009).

[16] R. Przyłucki, S. Golak, B. Oleksiak, L. Blacha, Influence of the geometry of the arrangement inductor-crucible to the velocity of the transport of mass in the liquid metallic phase mixed inductive, Archives of Civil and Mechanical Engineering **11** (1), 171-179 (2011).

[17] R. Przyłucki, Calculations of the induction heating system with the monitoring of thermal stress in the charge, Przegląd elektrotechniczny **84** (11), 210-214 (2008).

[18] T. Merder, Effect of casting flow rate on steel flow phenomena in tundish, Metalurgija **52** (2), 161-164 (2013).

[19] J. Barglik, D. Dolega, A. Smagor, Coupled temperature electromagnetic flow fields in the electromagnetic stirrer with a rotating magnetic field, Magnetohydrodynamics **46** (4), 387-392 (2010).

[20] S. Semiatin, V. Ivanchenko, S.O. Akhonin, O.M. Ivasishin, Diffusion models for evaporation losses during electron-beam melting of alpha/beta-titanium alloys, Metallurgical and Materials Transactions B **35 B**, 235-245 (2004).

Received: 13 May 2013.